Inorganic Chemistry

Article

pubs.acs.org/IC

Tuning the Electronic Structure of Fe(II) Polypyridines via Donor Atom and Ligand Scaffold Modifications: A Computational Study

David N. Bowman, Alexey Bondarev, Sriparna Mukherjee, and Elena Jakubikova*

Department of Chemistry, North Carolina State University, Raleigh, North Carolina 27695, United States

Supporting Information

ABSTRACT: Fe(II) polypyridines are an important class of pseudo-octahedral metal complexes known for their potential applications in molecular electronic switches, data storage and display devices, sensors, and dye-sensitized solar cells. Fe(II) polypyridines have a d^6 electronic configuration and pseudo-octahedral geometry and can therefore possess either a high-spin (quintet) or a low-spin (singlet) ground state. In this study, we investigate a series of complexes based on $[Fe(tpy)_2]^{2+}$ (tpy = 2,2′;6′,2″-terpyridine) and $[Fe(dcpp)_2]^{2+}$ (dcpp = 2,6-bis(2-carboxypyridyl)pyridine). The ligand field strength in these complexes is systematically tuned by replacing the central pyridine with five-membered (N-heterocyclic carbene, pyrrole, furan) or six-membered (aryl, thiazine-1,1-dioxide, 4-pyrone) moieties. To determine the impact of ligand substitutions on the relative energies of metal-centered states, the singlet, triplet, and quintet states of the Fe(II) complexes were optimized in water (PCM) using density functional theory at the B3LYP+D2 level with 6-311G* (nonmetals) and SDD (Fe) basis sets. It was found that the dcpp ligand scaffold allows for a more ideal octahedral coordination environment in comparison to the tpy ligand scaffold. The presence of six-membered central rings also allows for a more ideally octahedral coordination environment relative to five-membered central rings, regardless of the ligand scaffold. We find that the ligand field strength in the Fe(II) polypyridines can be tuned by altering the donor atom identity, with C donor atoms providing the strongest ligand field.

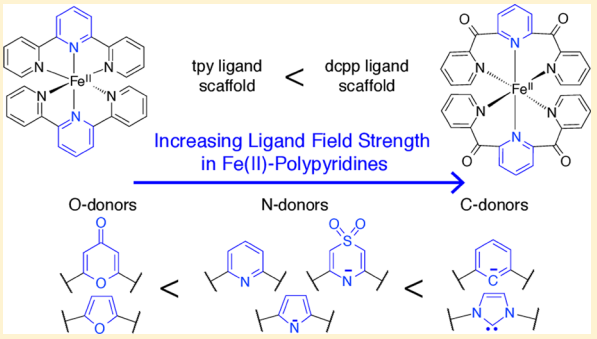

1. INTRODUCTION

Pseudo-octahedral Fe(II) complexes have a wide variety of potential applications due to their magnetic and photophysical properties. As a first-row transition metal, Fe provides for weak ligand field strength if used as a central metal in a coordination complex. Therefore, Fe compounds are characterized by the presence of a large number of electronic states with different multiplicities close to each other in energy. Depending on the ligand set utilized, energy ordering of the various electronic states can change and Fe(II) complexes with either a low-spin or a high-spin ground state can be prepared. This tunability makes iron compounds interesting as candidates for molecular memory,[1] pigments in display devices,[2] photosensitizers,[3] and other functional materials.[4] Fe(II) polypyridines are of particular interest for dye-sensitized solar cells[3,5] (DSSCs) and spin-crossover (SCO) materials.[4]

The Tanabe-Sugano diagram for d^6 octahedral complexes,[6] shown in Figure 1, is useful for understanding the changes to the relative energies of various metal-centered (MC) states present in Fe(II) complexes relative to the ligand field strength. For applications where bistability is important (e.g., switches and sensors), it is generally favorable to be near the SCO point (solid vertical line in Figure 1).[7] On the other hand, stabilization of the ^{1}A state is important for photovoltaic or photocatalytic applications, especially for tuning the lifetimes of the excited photoactive ligand-based charge-transfer states.[8−11] Fe(II) polypyridines often reside near the SCO point but can be pushed further into either the ^{1}A or ^{5}T stability regions by various ligand alterations.[12−19] External perturbations (e.g., pressure changes, solvent interactions) can also alter the relative stability of the states, but these phenomena apply to condensed matter systems that are beyond the scope of this study.[20−23]

Our particular interest in Fe(II) polypyridine complexes stems from their potential to serve as light harvesters in DSSCs. Fe(II) polypyridines are in many ways similar to the Ru(II) polypyridine compounds that have been successfully used as photosensitizers in DSSCs.[24] For example, visible light excitation in both ruthenium and iron polypyridine complexes results in $t_{2g} \rightarrow \pi^*$ transitions into a manifold of metal-to-ligand charge transfer (MLCT) states. These MLCT states are photoactive and can sensitize TiO_2 by undergoing interfacial electron transfer (IET) into the semiconductor. However, MLCT states are very short lived in Fe(II) polypyridines, as they undergo relaxation into the manifold of nonemissive high-spin metal-centered (MC) states on a subpicosecond time scale.[25] Thus, the main obstacle to the utilization of Fe(II)-based compounds as photosensitizers is the short lifetime of the initially populated MLCT states due to their deactivation by very fast intersystem crossing (ISC) events.[5,25−27]

Received: June 24, 2015
Published: August 21, 2015

DOI: 10.1021/acs.inorgchem.5b01409
Inorg. Chem. 2015, 54, 8786−8793

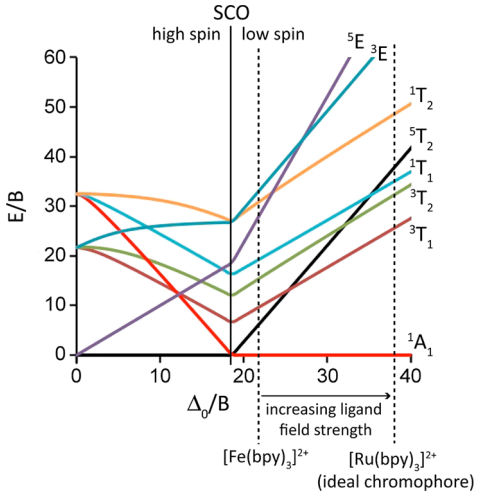

Figure 1. Simplified Tanabe–Sugano diagram for a d^6 complex with O_h symmetry. Δ_0 corresponds to the ligand field splitting parameters, and E denotes the energy. The values of Racah parameters used in preparing the diagram are B = 1080 cm^{-1} and C = 4774 cm^{-1}. Lowering of the symmetry of the complex to D_3, C_{2v}, or C_2 reduces the degeneracy of the triplet and quintet states shown in the diagram.[28,29]

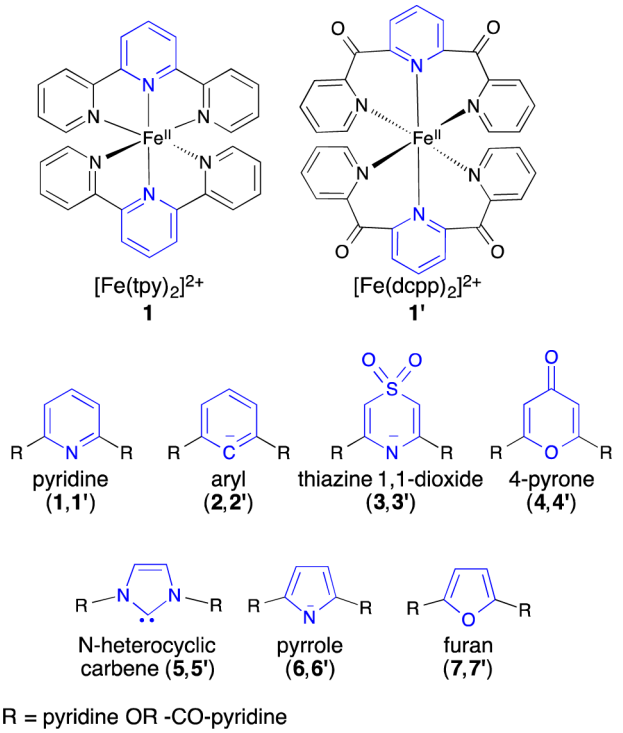

Figure 2. Complexes investigated in this study, which are based on the [Fe(tpy)$_2$]$^{2+}$ (**1**) and [Fe(dccp)$_2$]$^{2+}$ (**1′**) parent complexes. From these parent complexes, the central ring was replaced with the rings shown to produce complexes **2**–**7** (from **1**) and **2′**–**7′** (from **1′**).

In general, there are two possible approaches to increasing the efficiency of Fe(II) complexes as sensitizers. The first one tackles this problem by speeding up the rate of the IET, with the aim to make it more competitive with the ultrafast ISC process.[30,31] The second approach aims to slow down the ISC process by increasing the ligand field strength of Fe(II) polypyridines via ligand modifications. This can be achieved either via changing the character of the donor ligands themselves[8,10,11,32−34] or by changing the geometry of the ligand scaffold around the metal center.[9,35,36] The end goal is to increase the ligand field strength of Fe(II) polypyridines to the point where the ordering of various electronic states mirrors that of their Ru(II) analogues (see Figure 1).

The influence of donor atom and ligand scaffold modifications on the ligand field strength of a series of pseudooctahedral Fe(II) complexes (see Figure 2) was investigated in this work. Two closely related complexes, [Fe(tpy)$_2$]$^{2+}$ (**1**; tpy = 2,2′;6′,2″-terpyridine) and [Fe(dcpp)$_2$]$^{2+}$ (**1′**; dcpp = 2,6-bis(2-carboxypyridyl)pyridine), which contain the same set of pyridine donor ligands but differ in the choice of the pyridine connecting groups, were chosen as starting points for further modifications. While complex **1** has been previously studied and thoroughly characterized,[37−41] complex **1′** was synthesized only recently by McCusker and co-workers, who suggested that **1′** exhibits increased ligand field strength in comparison to **1**.[9] For complexes with tpy and dcpp scaffolds as the starting points, a series of systematic modifications was performed in which central pyridine rings are replaced with five-membered or six-membered rings with C, N, or O donor atoms. These studies served to evaluate the impact of the donor atom identity (C vs N vs O), ligand scaffold (tpy vs dcpp), and ring size (five-membered vs six-membered rings) on the ligand field strength of pseudo-octahedral Fe(II) complexes. Finally, a simple model system based on [Fe(NH$_3$)$_6$]$^{2+}$ was utilized to explore the influence of bond lengths and bond angles on the relative energetics of ^{1}A, ^{3}T$_1$, and ^{5}T$_2$ states in σ-donor octahedral FeL$_6$ complexes. Overall, computational studies presented in this work have helped us to define the range of ligand field strengths accessible for Fe(II) polypyridines and establish design principles for tuning the ligand fields in such complexes.

2. METHODOLOGY

The complexes shown in Figure 2, along with the [Fe(NH$_3$)$_6$]$^{2+}$ model system, were optimized in their singlet, triplet, and quintet states employing the B3LYP functional[42−45] with Grimme's D2 dispersion correction.[46] The SDD effective core potential (ECP) and associated basis set were used to describe the Fe center,[47] and the 6-311G* basis set was used for all other atoms (S, O, N, C, and H).[48,49] An ultrafine grid was used in all calculations. Solvent effects (water) were included in the calculations via a polarizable continuum model (PCM).[50] Vibrational frequency analysis was used to confirm that all optimized structures correspond to local minima on their respective potential energy surfaces. Natural orbital analysis was performed on open-shell systems to confirm metal-centered triplet and quintet states. All calculations were carried out employing the Gaussian 09 software package.[51]

The ground state multiplicity and relative ligand field strengths of all complexes were determined by comparison of calculated energy differences among quintet, triplet, and singlet states across all complexes, using an approach discussed in our previous work.[12] We have previously shown that while the accurate spin-state energetics is difficult to calculate with DFT, one can obtain reliable trends for the spin state energetics in a set of structurally related complexes.[12] Therefore, rather than aiming to obtain highly accurate energy differences among the singlet, quintet, and triplet metal-centered states investigated, we rely on the interpretation of trends across a set of structurally related complexes and utilize experimental benchmarks for comparison. [Fe(tpy)$_2$]$^{2+}$ and [Fe(dcpp)$_2$]$^{2+}$ complexes are both experimentally known to be singlets in their ground states and can therefore be used as benchmarks for ground-state determinations.[9,41] All complexes with the calculated quintet−singlet energy differences higher than those of the benchmark complexes are predicted to be singlets in their ground states.

DOI: 10.1021/acs.inorgchem.5b01409
Inorg. Chem. 2015, 54, 8786−8793

It should also be noted that our methodology was chosen with the aim to obtain reliable structures for both $[Fe(tpy)_2]^{2+}$ and $[Fe(dcpp)_2]^{2+}$ complexes and reasonable spin-state energetics for $[Fe(tpy)_2]^{2+}$.[12] For both species, the average percent error in the metal−ligand bond lengths was 2% and the percent errors in angles between metal−ligand bonds were all 1% or less relative to crystal structures. The calculated energy differences between singlet and quintet metal-centered states are 6.8 kcal/mol with B3LYP*[52] and 5.8 kcal/mol with B3LYP+D2, with the basis mentioned in the preceding paragraph. D2 dispersion correction was also included in the calculations, as it is needed to properly reproduce the crystal structure of $[Fe(dcpp)_2]^{2+}$, which displays van der Waals interactions between the carbonyl groups and pyridine rings on the opposing ligand. Images of optimized singlet structures along with the comparison to experimental crystal structures are given in Figure S1 and Table S1 in the Supporting Information.

Singlet, triplet, and quintet optimized structures of $[Fe(NH_3)_6]^{2+}$ were symmetrized to produce an ideal coordination environment by averaging all Fe−N bond lengths and setting N−Fe−N bite angles to either 90 or 180°. For the symmetrized singlet and quintet geometries, the coordination environment was set to O_h symmetry with Fe−N bond lengths of 2.064 Å (singlet) and 2.230 Å (quintet). The coordination environment for the symmetrized triplet geometry was set to D_{4h} symmetry with Fe−N bond lengths of 2.046 Å (axial N) and 2.197 Å (equatorial N). Potential energy surface (PES) scans were then performed on each of these systems with respect to the change in a single Fe−N bond length, all six Fe−N bond lengths, a single N−Fe−N bite angle (α), or both N−Fe−N bite angles (α), as shown in Figure 3. Fe−N bond lengths were varied by ±0.2 Å in steps of 0.05 Å.

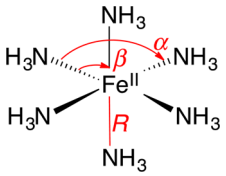

Figure 3. The model system $[Fe(NH_3)_6]^{2+}$ used to estimate the destabilization of singlet, triplet, and quintet states of the complexes studied by modulating the bite angles (α, β) and the metal−ligand bond length (R).

The N−Fe−N bite angles (α) were systematically reduced from 180 to 130° in steps of 10° (5° for each β). Hydrogens on all NH_3 ligands were fully relaxed at each point of the PES scan.

3. RESULTS AND DISCUSSION

The results are organized as follows. First, the influence of substitutions on the molecular structures of all complexes with tpy- and dcpp-based ligands in the ^{1}A state is described, followed by the analysis of the energy differences between their ^{1}A, ^{3}T, and ^{5}T MC states. Finally, a simplified $[Fe(NH_3)_6]^{2+}$ model system is used to illustrate how geometric distortions in the first coordination sphere alter energies of the ^{1}A, ^{3}T, and ^{5}T states.

3.1. Analysis of ^{1}A Structures of $[Fe(tpy)_2]^{2+}$- and $[Fe(dcpp)_2]^{2+}$-Based Systems. All iron(II) complexes investigated display pseudo-octahedral geometry in their singlet electronic state. The coordination environment of each complex has approximately C_{2v} symmetry and is characterized by four equivalent Fe−N equatorial bond lengths, two equivalent Fe−L (L = C, C$^-$, N, N$^-$, O) axial bond lengths, and two equivalent N−Fe−N bite angles (see Figure 4). The symmetry of the immediate coordination environment around the iron, which consists of the six donor atoms coordinated to the central iron atom, is very important in determining the ligand field strength in these complexes. In general, with all else being equal, distortions from the ideal octahedral environment reduce the metal−ligand orbital overlap and decrease the ligand field strength of a transition-metal complex.

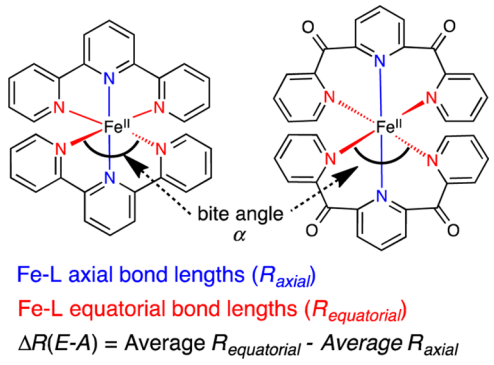

Figure 4. Geometric parameters describing the Fe−ligand coordination environment.

In order to quantify deviations from the ideal octahedral geometry, where ligand field splitting would be maximized, we have calculated the average N−Fe−N bite angles (α) and the differences in the average equatorial and axial Fe−L bond lengths, ΔR(E-A) (see Figure 4 and Table 1). For an ideally octahedral complex, the bite angles (α) would be precisely 180° and the differences between the average equatorial and axial bond lengths would be 0.

Table 1. Average Bite Angle (α, Figure 4) and Difference in Bond Lengths between Equivalent Sets of Metal−Ligand Bonds (ΔR(E-A), Figure 4) for Singlet States of Complexes 1−7 and 1′−7′, with Averages Based on Ligand Scaffold and Size of Central Ring[a]

complex	av bite angle α (deg)	ΔR(E−A) (Å)
ideal octahedral environment	180	0.00
$[Fe(tpy)_2]^{2+}$-based, six-membered central ring	161	0.08
$[Fe(tpy)_2]^{2+}$-based, five-membered central ring	154	0.20
$[Fe(dcpp)_2]^{2+}$-based, six-membered central ring	179	0.00
$[Fe(dcpp)_2]^{2+}$-based, five-membered central ring	177	0.09

[a]The average α and ΔR(E-A) values for each complex are given in Table S1 of the Supporting Information.

Two important trends can be seen from the data in Table 1. First, the substitution of five-membered rings into the tpy or dcpp ligand scaffold results in a significantly more distorted octahedral coordination environment relative to the complexes with six-membered central rings. The presence of the five-membered rings especially strains complexes based on the tpy scaffold, which display the most acute bite angles (154° on average). Second, the dcpp scaffold displays a more ideally octahedral coordination environment than the tpy scaffold. While the bite angles in tpy-based complexes range from 151 to 162°, bite angles in all dcpp-based complexes are between 175 and 179°, close to the ideal octahedral value of 180°. The observed structural trends are consistent with previous experimental work by McCusker and co-workers.[9]

3.2. Energy Ordering of ^{1}A, ^{5}T, and ^{3}T States in $[Fe(tpy)_2]^{2+}$- and $[Fe(dcpp)_2]^{2+}$-Based Systems. Electronic energy differences among the optimized ^{1}A, ^{3}T, and ^{5}T states

DOI: 10.1021/acs.inorgchem.5b01409
Inorg. Chem. 2015, 54, 8786−8793

were calculated for all complexes, in order to determine the relative energies of $^1A/^5T$ and $^3T/^5T$ electronic states, which reflect trends in the ligand field strength in this series of complexes. Note that DFT is not a reliable tool for calculations of energy differences between electronic states of various multiplicities, defined as

$$\Delta E_{HS/LS} = E_{high\text{-}spin} - E_{low\text{-}spin} \quad (1)$$

where $E_{high\text{-}spin}$ and $E_{low\text{-}spin}$ represent total energies of high-spin and low-spin states, respectively.[12,53] While an accurate determination of $\Delta E_{HS/LS}$ is difficult, we have previously shown that one can reliably determine trends is $\Delta E_{HS/LS}$ for a set of structurally related complexes.[12,53] Structurally related complexes are defined as those that undergo similar distortions in their metal–ligand bond lengths between the high-spin and low-spin structures, $\Delta R_{HS/LS}$, defined as

$$\Delta R_{HS/LS} = \sum_{i=1}^{n} \frac{R_i^{HS}}{n} - \sum_{i=1}^{n} \frac{R_i^{LS}}{n} \quad (2)$$

where R_i^{HS} and R_i^{LS} correspond to metal–ligand bond lengths at high-spin and low-spin optimized structures, respectively, and n is the total number of metal–ligand bonds in the transition-metal complex. For these structurally related complexes, $\Delta\Delta E_{HS/LS}$, defined as

$$\Delta\Delta E_{HS/LS} = \Delta E_{HS/LS}^{complex\ 1} - \Delta E_{HS/LS}^{complex\ 2} \quad (3)$$

has significantly reduced error relative to $\Delta E_{HS/LS}$, as all of the species suffer from the same systematic error in $\Delta E_{HS/LS}$. Please note that intermolecular interactions were not taken into account in our calculations. Such interactions can, in principle, influence the spin multiplicity of the ground electronic state.[54]

Average changes in the metal–ligand bond lengths calculated at singlet–quintet ($\Delta R_{Q/S}$), triplet–singlet ($\Delta R_{T/S}$), and triplet–quintet ($\Delta R_{Q/T}$) geometries for all of the complexes are shown in Table 2. Note that complex **5** undergoes a very large structural distortion in its quintet state, as demonstrated by disproportionately large $\Delta R_{Q/S}$ and $\Delta R_{Q/T}$ values in comparison to the rest of the complexes (its structure in ^5T is no longer pseudo-octahedral) and is therefore excluded from further analysis.

Considering the two sets of compounds based on tpy (**1**–**7**) and dcpp (**1′**–**7′**) scaffolds separately, complexes within each of the sets clearly undergo similar changes in the metal–ligand coordination environment for all pairs of high-spin/low-spin electronic states considered. Therefore, the trends in the calculated $\Delta E_{HS/LS}$ values within each set of complexes will be reliable. It is less obvious whether one can confidently compare the calculated $\Delta E_{HS/LS}$ values among the complexes based on different ligand scaffolds. This is especially true for singlet–quintet energy differences, since the average $\Delta R_{Q/S}$ values for tpy- and dcpp-based complexes differ by 0.07 Å. To ensure that the trends in $\Delta E_{Q/S}$ are reliable, we have calculated $\Delta E_{Q/S}$ values for complexes **1** and **1′** for 0–25% of exact exchange admixture in the B3LYP functional (see Figure 5). We found that the slopes of the $\Delta E_{Q/S}$ dependence on the exact exchange admixture are very similar for the two complexes. Moreover, $[Fe(dcpp)_2]^{2+}$ is predicted to possess stronger ligand field strength than $[Fe(tpy)_2]^{2+}$ at all levels of theory investigated (the energetic spacing between the scaffolds was found to be 3.1–6.9 kcal/mol over the investigated admixtures). Therefore, we conclude that we can employ the trends in $\Delta E_{HS/LS}$ obtained at the B3LYP level of theory to draw chemically relevant conclusions across this set of complexes.

Table 2. Changes in the Metal–Ligand Bond Lengths between the Quintet and Singlet ($\Delta R_{Q/S}$), Triplet and Singlet ($\Delta R_{T/S}$), and Quintet and Triplet ($\Delta R_{Q/T}$) States of Complexes 1–7 and 1′–7′[a]

complex	$\Delta R_{Q/S}$ (Å)	$\Delta R_{T/S}$ (Å)	$\Delta R_{Q/T}$ (Å)
1	0.217	0.099	0.119
2	0.263	0.120	0.143
3	0.187	0.095	0.092
4	0.215	0.098	0.117
5[b]	0.477	0.123	0.353
6	0.254	0.134	0.120
7	0.241	0.123	0.118
1′	0.153	0.076	0.077
2′	0.198	0.086	0.112
3′	0.147	0.080	0.067
4′	0.139	0.072	0.067
5′	0.187	0.087	0.100
6′	0.171	0.091	0.081
7′	0.150	0.070	0.080
1–**7** average (σ)	0.230 (0.026)	0.112 (0.015)	0.118 (0.015)
1′–**7′** average (σ)	0.164 (0.021)	0.080 (0.007)	0.083 (0.016)

[a]Average changes and standard deviations (σ) were also calculated for each set of complexes. [b]Complex **5** does not exhibit pseudo-octahedral coordination in quintet state and is therefore excluded from the calculated average.

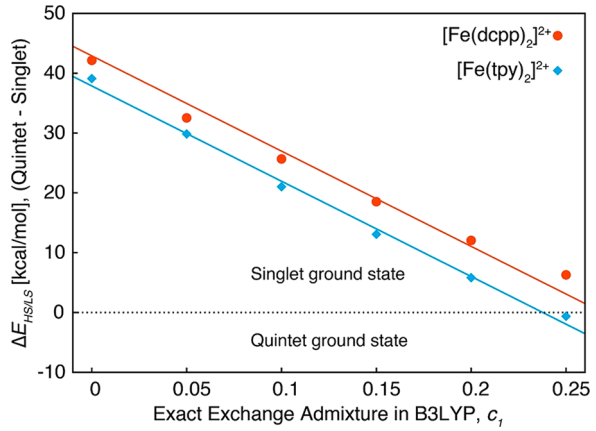

Figure 5. Plot of $\Delta E_{HS/LS}$ with respect to the exact exchange admixture (c_1) using the B3LYP functional with dispersion GD2 and SDD on Fe and 6-311G* basis set on all other atoms for complexes $[Fe(tpy)_2]^{2+}$ and $[Fe(dcpp)_2]^{2+}$. All of the optimizations were done using PCM as a model for water.[50] Linear fits with average slope of −150.47 kcal/mol give R^2 = 0.99 and 0.98 for $[Fe(tpy)_2]^{2+}$ and $[Fe(dcpp)_2]^{2+}$, respectively.

Comparing the $\Delta E_{HS/LS}$ values between the complexes, we can relate the changes in the geometric structure and the donor to the ligand field strength. We have plotted $\Delta E_{HS/LS}$ versus the identity of the central ring for both the tpy and dcpp scaffolds in Figure 6 ($\Delta E_{HS/LS} = E_{quintet} - E_{singlet}$) and Figure 7 ($\Delta E_{HS/LS} = E_{quintet} - E_{triplet}$). The ordering of the central rings in Figures 6 and 7 is based on the increasing stability of the singlet state relative to the quintet state, the two potential ground states for the tpy scaffold. The results show that the dcpp scaffold consistently stabilizes the lower-spin states for all complexes. For singlet/quintet states the average stabilization of the singlet state is 11.8 kcal/mol, and for the triplet/quintet states the

DOI: 10.1021/acs.inorgchem.5b01409
Inorg. Chem. 2015, 54, 8786–8793

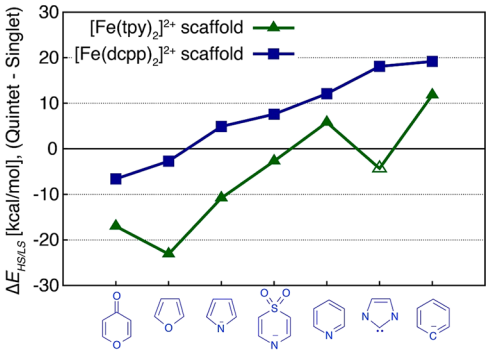

Figure 6. Plot of $\Delta E_{HS/LS}$ between the quintet and singlet states for the $[Fe(tpy)_2]^{2+}$-based (green line) and $[Fe(dcpp)_2]^{2+}$-based (blue line) complexes versus the identity of the central ring.

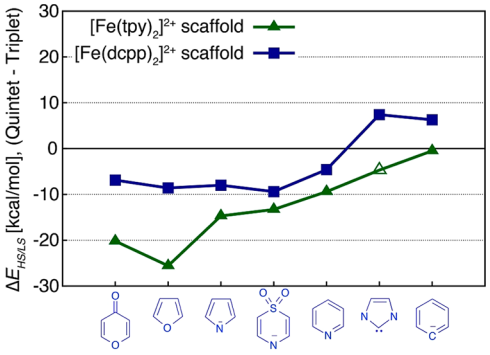

Figure 7. Plot of $\Delta E_{HS/LS}$ between the quintet and triplet states for the $[Fe(tpy)_2]^{2+}$-based (green line) and $[Fe(dcpp)_2]^{2+}$-based (blue line) complexes versus the identity of the central ring.

average stabilization of the triplet state is 8.8 kcal/mol (excluding **6** and **6′**).

The most reliable comparison of ligand field strengths from these results is $\Delta\Delta E_{HS/LS}$, the energy difference between $\Delta E_{HS/LS}$ values of complexes with varying ligand scaffold or central ring identity. We must, however, exclude the $\Delta E_{HS/LS}$ values for complex **5** (N-heterocyclic carbene ring substituted into the tpy scaffold) from all comparisons, due to the strained structure of the quintet state as previously mentioned. The $\Delta\Delta E^{scaffold}_{HS/LS}$ value, defined as the difference between $\Delta E_{HS/LS}$ of complexes with the tpy and dcpp ligand scaffolds containing the same set of ligands, is largest for the systems with five-membered central rings, reflecting that the use of the dcpp scaffold results in a more ideal coordination environment for smaller central rings. On average, the value of $\Delta\Delta E^{scaffold}_{HS/LS}$ is 8.6 kcal/mol for six-membered central ring systems and 18.0 kcal/mol for systems with five-membered rings for the singlet quintet energy differences shown in Figure 6 (excluding complexes **6** and **6′**). These trends can be attributed to (1) the geometric conformation of the bound tpy scaffold versus the dcpp scaffold and (2) electronic effects arising from the differences in **1** and **1′**. Use of the dcpp scaffold consistently leads to a more ideally octahedral coordination environment than the tpy scaffold. Overall, we find that the dcpp scaffold affords stronger-field ligands than the tpy scaffold and should be considered when stabilization of a singlet ground state is desired. The effect of geometric distortions away from the ideal octahedral coordination environment will be discussed further in section 3.3, using a model system based on $[Fe(NH_3)_6]^{2+}$ where changes to the electronic structure are expected to be insignificant.

For the ground-state calculations, shown in Figure 6, we find that the ordering of donor atoms based on increasing ligand field strength is O < N < C, regardless of the ligand scaffold. The same trend is observed in Figure 7, in which increasing ligand field strength favors the triplet state over the quintet state, when the dcpp scaffold is utilized. On the basis of an analysis of metal-centered state splitting in an octahedral field by Tanabe and Sugano (also see Figure 1),[6] increasing ligand field strength should monotonically increase the $\Delta E_{HS/LS}$ value between the lowest energy quintet and singlet states as well as the quintet and triplet states. This trend is seen in both Figures 6 and 7, with slight deviations attributed to distortions away from the ideally octahedral coordination environment. It should be noted that considering $\Delta H_{HS/LS}$ or $\Delta G_{HS/LS}$ will lead to the same conclusions, as shown in Figures S2–S5 in the Supporting Information. All energy differences are tabulated in Tables S2 and S3 in the Supporting Information.

3.3. Effect of Structural Distortions in $[Fe(NH_3)_6]^{2+}$ Model System. A simplified model system, the hexaammineiron(II) cation ($[Fe(NH_3)_6]^{2+}$), was used to determine how structural distortions of the metal–ligand environment alter the energy of the relevant metal-centered states. This model system is useful for two reasons. (1) The use of NH_3 ligands helps us to isolate the impact of structure on σ-donation effects only, since NH_3 is a pure σ donor. This is useful in terms of understanding bonding in polypyridine-based ligands as well, because they act primarily as σ donors and are, at best, weak π acceptors.[55] (2) Several high-level ab initio calculations and previous DFT studies are known in the literature that can serve as benchmarks for our calculations.[56,57]

Bite angles (α) and Fe–N bond lengths for the singlet, triplet, and quintet metal-centered states of this complex were systematically distorted, as diagrammed in Figure 3. The initial structures were symmetrized versions of the fully relaxed geometries. For the singlet and quintet states, the symmetrized Fe–N environment has O_h symmetry with Fe–N bond lengths of 2.064 and 2.230 Å, respectively. An asymmetric population of the e_g metal orbitals in the triplet state leads to a significant Jahn–Teller distortion of the bond lengths. The symmetrized triplet state has a Fe–N environment of D_{4h} symmetry with bond lengths of 2.046 Å (axial) and 2.197 Å (equatorial). All symmetrized structures have negligible energy differences, ranging from 0.2 to 0.7 kcal/mol, relative to the fully optimized systems.

The quantity of interest for the model system is the destabilization energy due to distortions away from the symmetrized geometry, defined as

$$\Delta E_D = E_{dist} - E_{symm} \quad (4)$$

where E_{dist} and E_{symm} refer to distorted and symmetrized structures, respectively. It is also useful to look at destabilization energy relative to the energy of the symmetrized quintet, which is the lowest energy structure

$$\Delta E_{D,q} = E_{dist} - E_{symm,quin} \quad (5)$$

where $E_{symm,quin}$ refers to the symmetrized quintet structure. A plot of ΔE_D for singlet, triplet, and quintet spin states versus the distortion of the Fe–N bonds (both one bond and all six bonds) is shown in Figure 8.a, along with a plot of $\Delta E_{D,q}$ versus the average Fe–N bond length for the same states (all six

DOI: 10.1021/acs.inorgchem.5b01409
Inorg. Chem. 2015, 54, 8786–8793

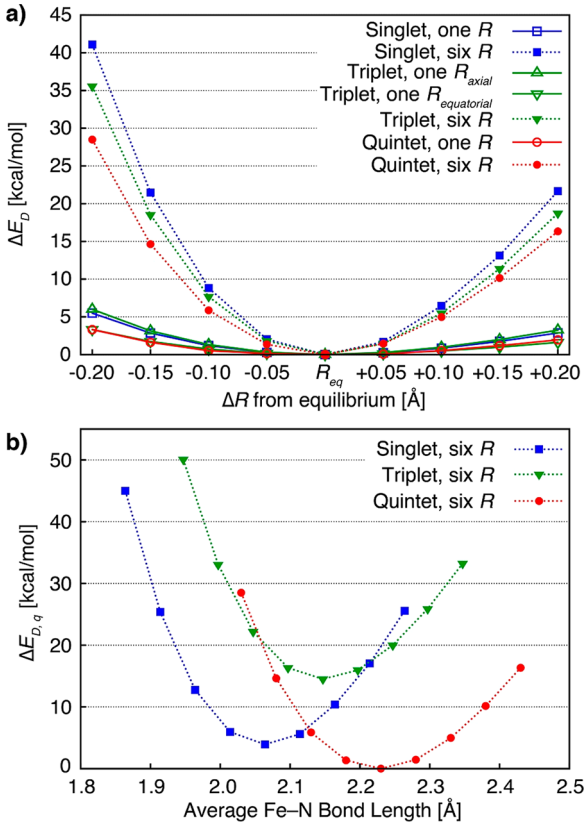

Figure 8. (a) Plot of destabilization energy, ΔE_D, for singlet (blue), triplet (green), and quintet (red) states of $[Fe(NH_3)_6]^{2+}$ versus the distortion of one Fe−N bond (solid lines) or six Fe−N bonds (dashed lines). The N−Fe−N bite angle α was held constant at 180°, and R_{eq} = 2.064 Å (singlet), 2.046 Å (triplet, axial), 2.197 Å (triplet, equatorial), and 2.230 Å (quintet). (b) Plot of destabilization energies relative to the lowest energy of the quintet state, $\Delta E_{D,q}$, versus the average Fe−N bond length in the $[Fe(NH_3)_6]^{2+}$ system. Note that while equatorial and axial Fe−N bond lengths are identical in structures used for singlet and quintet states, the average Fe−N bond length for the triplet state represents an average of equatorial and axial bonds, which always differ by 0.151 Å in the D_{4h} structure.

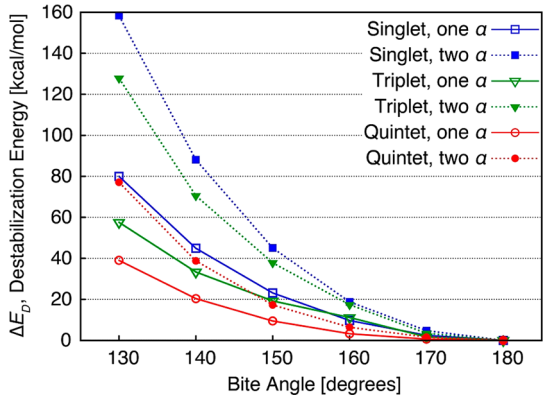

Figure 9. Plot of destabilization energy, ΔE_D, for singlet (blue), triplet (green), and quintet (red) states of $[Fe(NH_3)_6]^{2+}$ versus the contraction of one N−Fe−N bite angle α (solid lines) and both N−Fe−N bite angles α (dashed lines). The Fe−N distances correspond to the symmetrized equilibrium bond lengths (R_{eq}) given in the caption of Figure 8.

bonds distorted). In Figure 8.b, potential energy surfaces for the states along the average metal−ligand bond length coordinate are plotted. It should be noted that on the basis of previous highly accurate ab initio calculations, the expected energy difference between the quintet and singlet states should be in the range of approximately 20−32 kcal/mol (with quintet being the lowest energy state), which we underestimate by at least 15 kcal/mol.[56,57] This is not entirely surprising, as the character of metal−ligand bonds in this species is more ionic than that in the polypyridines and one would therefore need to use a functional with an increased amount of exact exchange to accurately determine its spin-state energetics.[12] The chosen methodology, however, provides us with useful qualitative insights, and errors in the vertical displacement of different spin states along the energy axis of Figure 8.b do not affect the major conclusions drawn.

The destabilization energy relative to the state of interest (ΔE_D) versus the N−Fe−N bite angles (α) for these states is given in Figure 9, in which one or two α angles are changed. It is important to note that, for this system, bite angle and bond length distortions to the symmetrized structure can be performed independently in a straightforward manner. For chelating ligands, such as tpy, independent distortions to these geometric parameters are complicated by significant deviations from O_h symmetry in the optimized Fe−N environments.

The destabilization energies for both structures distorted either by changes to all Fe−N bond lengths (see Figure 8a) or both N−Fe−N bite angles (see Figure 9) show important trends among the metal-centered states investigated. The magnitude of the destabilization energy is consistently greater for lower spin states (or states with a smaller number of unpaired electrons), in the order singlet > triplet > quintet. Due to the electronic properties of FeN_6 systems with relatively sterically unhindered ligands,[58,59] the curvature of the potential energy surface (PES) also follows the same trend. This can be explained by the fact that higher multiplicity metal-centered states of these systems have one or two antibonding e_g orbitals populated, which results in weaker Fe−N bonds. The weaker bonds have both (1) a longer equilibrium bond distance and (2) a shallower PES along the Fe−N coordinate (see Figure 8). From Figure 8b, destabilization energy relative to the quintet state, it is clear that the singlet state is the most stable state at average Fe−N lengths of less than approximately 2.12 Å and for longer bond lengths the quintet state is the most stable state.

An additional feature of the destabilization energies for all spin states and both kinds of distortions considered is that the total destabilization (from perturbing all six bonds or both bite angles) is additive. Thus, we can conclude that each distortion is independently contributing to the overall destabilization energies of the various states, and the total destabilization energy is simply a sum of the individual contributions. The additive nature of the destabilization energy is not expected to hold in general. In the case that a complex has negligible electronic communication through the metal center and sterically unhindered ligands, additive destabilization may be expected.

It is difficult to compare the destabilization trends from Fe−N bond length changes (Figure 8) with those resulting from decreased bite angle (Figure 9), as these geometric parameters are distinctly different. In general, however, a chemist will have flexibility to change bite angles, for example through ligand scaffold design,[9] and equilibrium bond lengths via steric interactions.[3,5,60] It is obvious that the bite angle has a drastic effect on the destabilization energy of the model system and

DOI: 10.1021/acs.inorgchem.5b01409
Inorg. Chem. 2015, 54, 8786−8793

that these distortions will cause the higher spin states to become stabilized relative to the singlet state when metal−ligand bond lengths are fixed. For the family of $[Fe(tpy)_2]^{2+}$-based complexes investigated, the significant distortion of their bite angles (161° on average, see Table 1) from the ideal octahedral environment is certainly important when considering future ligand design.

For designing Fe(II) complexes with stable singlet ground states and relatively destabilized metal-centered excited states, maintaining a nearly ideal O_h coordination environment (as with the dcpp scaffold) is certainly an important factor to consider. Formation of carbon−iron bonds is also suggested for maximizing the ligand field strength. Future work will be focused on investigating further modifications to the dcpp scaffold, including changing the identity of the carbonyl group joining the pyridine moieties and replacement of the side pyridine rings.

4. CONCLUSIONS

In this work a series of systems based on $[Fe(tpy)_2]^{2+}$ and $[Fe(dcpp)_2]^{2+}$ with central pyridine rings substituted by five-membered (N-heterocyclic carbene, pyrrole, furan) or six-membered (aryl, thiazine-1,1-dioxide, 4-pyrone) moieties was considered. The aim of this work was to elucidate fundamental principles for ligand design allowing one to tune the ligand field strength of Fe(II) polypyridines. We find that the use of a dcpp scaffold allows for a significant increase of the ligand field strength of Fe(II) complexes as well as a more ideal octahedral coordination environment in comparison to the tpy scaffold. Additionally, we find a clear trend in the effect of the donor atom identity on the resulting ligand field strength. The N-heterocyclic carbene and aryl ring, both with a C donor atom, provide for the strongest ligand fields regardless of the ligand scaffold. Nitrogenous heterocyclic rings provide for moderate ligand field strength, while oxygen-based heterocycles result in the weakest field strength.

A model system based on $[Fe(NH_3)_6]^{2+}$ was utilized to obtain a better understanding of the energetic destabilization effects caused by deviations from an ideal octahedral coordination environment in Fe(II) complexes. From systematic distortions of the Fe−N bond lengths and N−Fe−N bite angles from their respective equilibrium geometries, we find that the singlet state is always the most destabilized state relative to the higher spin states. In particular, for applications of Fe(II) polypyridines as chromophores, the following design criteria seem to be of utmost importance: (1) the presence of Fe−C bonds in the system, (2) an ideal octahedral environment, and (3) short metal−ligand bond lengths. Overall, these design principles aid in elucidating what ligand field strengths should be achievable for Fe(II) polypyridines and determining how these ranges could be explored via structural modification.

■ ASSOCIATED CONTENT

Supporting Information

The Supporting Information is available free of charge on the ACS Publications website at DOI: 10.1021/acs.inorgchem.5b01409.

Images of optimized **1** and **1′** ground state singlet structures and relevant geometric parameters in comparison to crystal structure data, plots of enthalpy differences and Gibbs free energy differences between quintet and singlet and between quintet and triplet states of **1**−**7** and **1′**−**7′**, energy differences ($\Delta E_{HS/LS}$, $\Delta H_{HS/LS}$, $\Delta G_{HS/LS}$) between quintet/singlet and quintet/triplet states of **1**−**7** and **1′**−**7′**, average bite angles and differences in equatorial and axial bond lengths for all singlet states of **1**−**7** and **1′**−**7′**, and expectation value of $\langle S^2 \rangle$ for all triplet and quintet states of **1**−**7** and **1′**−**7′** (PDF)

Cartesian coordinate file of optimized singlet, triplet, and quintet structures of **1**-**7** and **1′**-**7′**, and symmetrized $[Fe(NH_3)_6]^{2+}$ singlet, triplet, and quintet structures (XYZ)

■ AUTHOR INFORMATION

Corresponding Author

*E-mail for E.J.: ejakubi@ncsu.edu.

Notes

The authors declare no competing financial interest.

■ ACKNOWLEDGMENTS

We gratefully acknowledge support from the U.S. Army Research Office under contract number W911NF-15-1-0124. D.N.B. also acknowledges support from the U.S. Department Of Education Graduate Assistantship In Areas Of National Need (GAANN) Fellowship Program at North Carolina State University.

■ REFERENCES

(1) Gütlich, P.; Garcia, Y.; Woike, T. *Coord. Chem. Rev.* **2001**, *219*−*221*, 839−879.
(2) Letard, J. F.; Guionneau, P.; Goux-Capes, L. *Spin Crossover in Transition Metal Compounds III* **2004**, *235*, 221−249.
(3) Ferrere, S.; Gregg, B. A. *J. Am. Chem. Soc.* **1998**, *120*, 843−844.
(4) Miller, J. S. Spin-Crossover Materials. In *Encyclopedia of Smart Materials*; Wiley: Hoboken, NJ, 2002.
(5) Monat, J. E.; McCusker, J. K. *J. Am. Chem. Soc.* **2000**, *122*, 4092−4097.
(6) Tanabe, Y.; Sugano, S. *J. Phys. Soc. Jpn.* **1954**, *9*, 766−779.
(7) Gütlich, P.; Goodwin, H. A. *Spin Crossover in Transition Metal Compounds I-III* **2004**, 1.
(8) Liu, Y.; Harlang, T.; Canton, S. E.; Chabera, P.; Suarez-Alcantara, K.; Fleckhaus, A.; Vithanage, D. A.; Goransson, E.; Corani, A.; Lomoth, R.; Sundstrom, V.; Warnmark, K. *Chem. Commun.* **2013**, *49*, 6412−6414.
(9) Jamula, L. L.; Brown, A. M.; Guo, D.; McCusker, J. K. *Inorg. Chem.* **2014**, *53*, 15−17.
(10) Dixon, I. M.; Alary, F.; Boggio-Pasqua, M.; Heully, J. L. *Inorg. Chem.* **2013**, *52*, 13369−13374.
(11) Dixon, I. M.; Khan, S.; Alary, F.; Boggio-Pasqua, M.; Heully, J. L. *Dalton T.* **2014**, *43*, 15898−15905.
(12) Bowman, D. N.; Jakubikova, E. *Inorg. Chem.* **2012**, *51*, 6011−6019.
(13) Real, J. A.; Gaspar, A. B.; Munoz, M. C. *Dalton T.* **2005**, 2062−2079.
(14) Gütlich, P.; Hauser, A. *Coord. Chem. Rev.* **1990**, *97*, 1−22.
(15) Hauser, A. *J. Chem. Phys.* **1991**, *94*, 2741.
(16) Halcrow, M. A. *Chem. Soc. Rev.* **2008**, *37*, 278−289.
(17) Decurtins, S.; Gütlich, P.; Köhler, C.; Spiering, H.; Hauser, A. *Chem. Phys. Lett.* **1984**, *105*, 1−4.
(18) Gütlich, P.; Garcia, Y.; Goodwin, H. A. *Chem. Soc. Rev.* **2000**, *29*, 419−427.
(19) Gütlich, P.; Hauser, A.; Spiering, H. *Angew. Chem., Int. Ed. Engl.* **1994**, *33*, 2024−2054.
(20) Tsuchiya, N.; Tsukamoto, A.; Ohshita, T.; Isobe, T.; Senna, M.; Yoshioka, N.; Inoue, H. *Solid State Sci.* **2001**, *3*, 705−714.
(21) Ni, Z.; McDaniel, A. M.; Shores, M. P. *Chem. Sci.* **2010**, *1*, 615−621.
(22) Ni, Z.; Shores, M. P. *J. Am. Chem. Soc.* **2009**, *131*, 32−33.

DOI: 10.1021/acs.inorgchem.5b01409
Inorg. Chem. 2015, 54, 8786−8793

(23) Schulte, K. A.; Fiedler, S. R.; Shores, M. P. *Aust. J. Chem.* **2014**, *67*, 1595−1600.
(24) Ardo, S.; Meyer, G. J. *Chem. Soc. Rev.* **2009**, *38*, 115−164.
(25) Smeigh, A. L.; Creelman, M.; Mathies, R. A.; McCusker, J. K. *J. Am. Chem. Soc.* **2008**, *130*, 14105−14107.
(26) Huse, N.; Cho, H.; Hong, K.; Jamula, L.; de Groot, F. M. F.; Kim, T. K.; McCusker, J. K.; Schoenlein, R. W. *J. Phys. Chem. Lett.* **2011**, *2*, 880−884.
(27) Juban, E. A.; Smeigh, A. L.; Monat, J. E.; McCusker, J. K. *Coord. Chem. Rev.* **2006**, *250*, 1783−1791.
(28) Jørgensen, C. K.; Jørgensen, C. *Modern Aspects of Ligand Field Theory*; North-Holland: Amsterdam, London, 1971.
(29) Atanasov, M.; Daul, C. A.; Rauzy, C. *Chem. Phys. Lett.* **2003**, *367*, 737−746.
(30) Bowman, D. N.; Mukherjee, S.; Barnes, L. J.; Jakubikova, E. *J. Phys.: Condens. Matter* **2015**, *27*, 134205.
(31) Jakubikova, E.; Bowman, D. N. *Acc. Chem. Res.* **2015**, *48*, 1441−1449.
(32) Fredin, L. A.; Pápai, M.; Rozsályi, E.; Vankó, G.; Wärnmark, K.; Sundström, V.; Persson, P. *J. Phys. Chem. Lett.* **2014**, *5*, 2066−2071.
(33) Dixon, I. M.; Alary, F.; Boggio-Pasqua, M.; Heully, J.-L. *Dalton Trans.* **2015**, *44*, 13498−13503.
(34) Mukherjee, S.; Bowman, D. N.; Jakubikova, E. *Inorg. Chem.* **2015**, *54*, 560−569.
(35) Mengel, A. K. C.; Förster, C.; Breivogel, A.; Mack, K.; Ochsmann, J. R.; Laquai, F.; Ksenofontov, V.; Heinze, K. *Chem. - Eur. J.* **2015**, *21*, 704−714.
(36) Liu, Y.; Kjær, K. S.; Fredin, L. A.; Chábera, P.; Harlang, T.; Canton, S. E.; Lidin, S.; Zhang, J.; Lomoth, R.; Bergquist, K.-E.; Persson, P.; Wärnmark, K.; Sundström, V. *Chem. - Eur. J.* **2015**, *21*, 3628−3639.
(37) Cho, H.; Strader, M. L.; Hong, K.; Jamula, L.; Gullikson, E. M.; Kim, T. K.; de Groot, F. M. F.; McCusker, J. K.; Schoenlein, R. W.; Huse, N. *Faraday Discuss.* **2012**, *157*, 463−474.
(38) Creutz, C.; Chou, M.; Netzel, T. L.; Okumura, M.; Sutin, N. *J. Am. Chem. Soc.* **1980**, *102*, 1309−1319.
(39) Braterman, P. S.; Song, J. I.; Peacock, R. D. *Inorg. Chem.* **1992**, *31*, 555−559.
(40) Constable, E. C.; Baum, G.; Bill, E.; Dyson, R.; van Eldik, R.; Fenske, D.; Kaderli, S.; Morris, D.; Neubrand, A.; Neuburger, M.; Smith, D. R.; Wieghardt, K.; Zehnder, M.; Zuberbühler, A. D. *Chem. - Eur. J.* **1999**, *5*, 498−508.
(41) Baker, A. T.; Goodwin, H. A. *Aust. J. Chem.* **1985**, *38*, 207−214.
(42) Becke, A. D. *J. Chem. Phys.* **1993**, *98*, 5648−5652.
(43) Becke, A. D. *Phys. Rev. A: At., Mol., Opt. Phys.* **1988**, *38*, 3098−3100.
(44) Stephens, P.; Devlin, F. *J. Phys. Chem.* **1994**, *98*, 11623−11627.
(45) Lee, C.; Yang, W.; Parr, R. G. *Phys. Rev. B: Condens. Matter Mater. Phys.* **1988**, *37*, 785−789.
(46) Grimme, S. *J. Comput. Chem.* **2006**, *27*, 1787−1799.
(47) Kaupp, M.; Schleyer, P. V.; Stoll, H.; Preuss, H. *J. Chem. Phys.* **1991**, *94*, 1360−1366.
(48) Krishnan, R.; Binkley, J. S.; Seeger, R.; Pople, J. A. *J. Chem. Phys.* **1980**, *72*, 650−654.
(49) Mclean, A. D.; Chandler, G. S. *J. Chem. Phys.* **1980**, *72*, 5639−5648.
(50) Scalmani, G.; Frisch, M. J. *J. Chem. Phys.* **2010**, *132*, 114110.
(51) Frisch, M. J.; Trucks, G. W.; Schlegel, H. B.; Scuseria, G. E.; Robb, M. A.; Cheeseman, J. R.; Scalmani, G.; Barone, V.; Mennucci, B.; Petersson, G. A.; Nakatsuji, H.; Caricato, M.; Li, X.; Hratchian, H. P.; Izmaylov, A. F.; Bloino, J.; Zheng, G.; Sonnenberg, J. L.; Hada, M.; Ehara, M.; Toyota, K.; Fukuda, R.; Hasegawa, J.; Ishida, M.; Nakajima, T.; Honda, Y.; Kitao, O.; Nakai, H.; Vreven, T.; Montgomery, J. A., Jr.; Peralta, J. E.; Ogliaro, F.; Bearpark, M.; Heyd, J. J.; Brothers, E.; Kudin, K. N.; Staroverov, V. N.; Kobayashi, R.; Normand, J.; Raghavachari, K.; Rendell, A.; Burant, J. C.; Iyengar, S. S.; Tomasi, J.; Cossi, M.; Rega, N.; Millam, J. M.; Klene, M.; Knox, J. E.; Cross, J. B.; Bakken, V.; Adamo, C.; Jaramillo, J.; Gomperts, R.; Stratmann, R. E.; Yazyev, O.; Austin, A. J.; Cammi, R.; Pomelli, C.; Ochterski, J. W.; Martin, R. L.; Morokuma, K.; Zakrzewski, V. G.; Voth, G. A.; Salvador, P.; Dannenberg, J. J.; Dapprich, S.; Daniels, A. D.; Farkas, Ö.; Foresman, J. B.; Ortiz, J. V.; Cioslowski, J.; Fox, D. J. *Gaussian 09, Revision D.01*; Gaussian, Inc., Wallingford, CT, 2009.
(52) Reiher, M.; Salomon, O.; Hess, B. A. *Theor. Chem. Acc.* **2001**, *107*, 48−55.
(53) Reiher, M. *Inorg. Chem.* **2002**, *41*, 6928−6935.
(54) Zerara, M.; Hauser, A. *ChemPhysChem* **2004**, *5*, 395−399.
(55) Leyssens, T.; Peeters, D.; Orpen, A. G.; Harvey, J. N. *Organometallics* **2007**, *26*, 2637−2645.
(56) Pierloot, K.; Vancoillie, S. *J. Chem. Phys.* **2006**, *125*, 124303.
(57) Fouqueau, A.; Casida, M. E.; Daku, L. M. L.; Hauser, A.; Neese, F. *J. Chem. Phys.* **2005**, *122*, 044110.
(58) de Graaf, C.; Sousa, C. *Chem. - Eur. J.* **2010**, *16*, 4550−4556.
(59) Sousa, C.; de Graaf, C.; Rudavskyi, A.; Broer, R.; Tatchen, J.; Etinski, M.; Marian, C. M. *Chem. - Eur. J.* **2013**, *19*, 17541−17551.
(60) Lin, H. J.; Siretanu, D.; Dickie, D. A.; Subedi, D.; Scepaniak, J. J.; Mitcov, D.; Clerac, R.; Smith, J. M. *J. Am. Chem. Soc.* **2014**, *136*, 13326−13332.

DOI: 10.1021/acs.inorgchem.5b01409
Inorg. Chem. 2015, 54, 8786−8793